Valley degree of freedom in ferromagnetic Janus monolayer H-VSSe and the asymmetry-based tuning of the valleytronic properties

Chaobo Luo, Xiangyang Peng,* Jinfeng Qu, and Jianxin Zhong
Hunan Key Laboratory for Micro-Nano Energy Materials and Devices, School of Physics and Optoelectronics, Xiangtan University, Hunan 411105, People's Republic of China

(Received 18 December 2019; revised manuscript received 29 May 2020; accepted 1 June 2020; published 15 June 2020)

By using density-functional theory-based GW method, we studied the valley degree of freedom of Janus monolayer VSSe. The GW corrections lead to a doubling of the band gap and change the band dispersion considerably, indicating significant many-body effects. VSSe is confirmed to be ferromagnetic, which breaks the time-reversal symmetry and the odd parity of the Berry curvature in momentum space. The dissimilar magnitudes of Berry curvatures of the inequivalent valleys give rise to appreciable anomalous Hall conductivity (AHC). The calculated valley optical response of VSSe exhibits a clear valley-selective circular dichroism. The ferromagnetism induces large valley-Zeeman splitting, making it possible to realize the selective valley excitation even by *unpolarized* light. The Janus VSSe is more tunable by external fields because of symmetry breaking. Due to the relief of time-reversal symmetry, the valley-Zeeman splitting can be continuously tuned by varying the magnetization direction. The loss of mirror symmetry in VSSe enables a bidirection modulation of the band gap by changing the direction of electric field. The strain can linearly tune the valley gap in a considerable range. The Berry curvature and AHC can be effectively regulated in the external fields.

DOI: 10.1103/PhysRevB.101.245416

I. INTRODUCTION

Transition-metal dichalcogenides (TMDs) have become a prominent family of two-dimensional materials. As an analog to graphene, it surpasses graphene in possessing direct band gap in visible light range and strong spin-orbit coupling, making TMDs excellent candidates for optical, electronic, spintronic, and photovoltaic applications [1–5]. The well-known representative members of TMDs are monolayer MX_2 ($M =$ Mo, W; $X =$ S, Se), in which there is a central M sublayer sandwiched by two mirror-symmetric X sublayers. Due to the lack of inversion symmetry, the H-MX_2 has a new degree of freedom, i.e., valley, which is coupled with spin degree of freedom to exhibit extraordinary quantum effects such as valley-spin locking and valley-spin Hall effect [6–14]. Recently, vanadium dichalcogenides H-VX_2 ($X =$ S, Se, Te) are arising as a distinguished group among the TMDs by being simultaneously semiconducting and ferromagnetic [15–18]. Two-dimensional ferromagnetic semiconductors are under intensive research for their superior potential in spintronics. The intrinsic ferromagnetism is further coupled with the valley degree of freedom in VX_2 to make a ferrovalley material [15].

Monolayer MXX' is a Janus variant of TMDs, in which the two chalcogen layers are different and hence the mirror symmetry existing in MX_2 is broken [19–21]. Ordered Janus MXX' has been synthesized by modified chemical vapor deposition (CVD) methods under careful control to avoid the formation of random alloys [19,22,23]. The out-of-plane asymmetry between the X and X' layers can significantly enhance the perpendicular piezoelectric effect. Janus VXX', in particular Janus monolayer H-VSSe (briefed as VSSe in the following), has also been studied recently [24,25]. It can be expected that ordered VSSe can be grown by the similar modified CVD methods as mentioned above. It is found that VSSe is strongly piezoelectric and multiferroic with strong ferroelasticity and ferromagnetism. Therefore, VSSe is expected to provide a unique platform to explore the electronic, optical, magnetic, and valleytronic properties and their synergistic effects. However, the coupling of the ferromagnetism and valleytronic properties in VSSe has not been explored. It is still to know how the effective magnetic field induced by ferromagnetism would affect the Berry curvatures, the related optical dichroism, and the anomalous Hall conductivity (AHC). The valley gaps have great effect on the electrical, optical, and valleytronic properties. The conventional density-functional theory calculations of vanadium dichalcogenides up to now did not consider the many-body effects and hence usually significantly underestimated the energy gap, which in turn would compromise the calculations of Berry curvatures, photoluminescence spectrum, AHC, etc.. In this study, we investigated the combining effects of magnetic exchange field and valleytronic properties in VSSe based on more rigorous quasiparticle GW method. The Berry phase-related quantum phenomena were examined.

In symmetrically equivalent directions, the response of the system to the external perturbations are identical. In MX_2, for instance, the electric fields along the two opposite perpendicular directions, which are equivalent due to the mirror symmetry between the two X layers, will have the same effect. With the breaking of the time-reversal symmetry, inversion symmetry, and mirror symmetry, VSSe should be

*xiangyang_peng@xtu.edu.cn

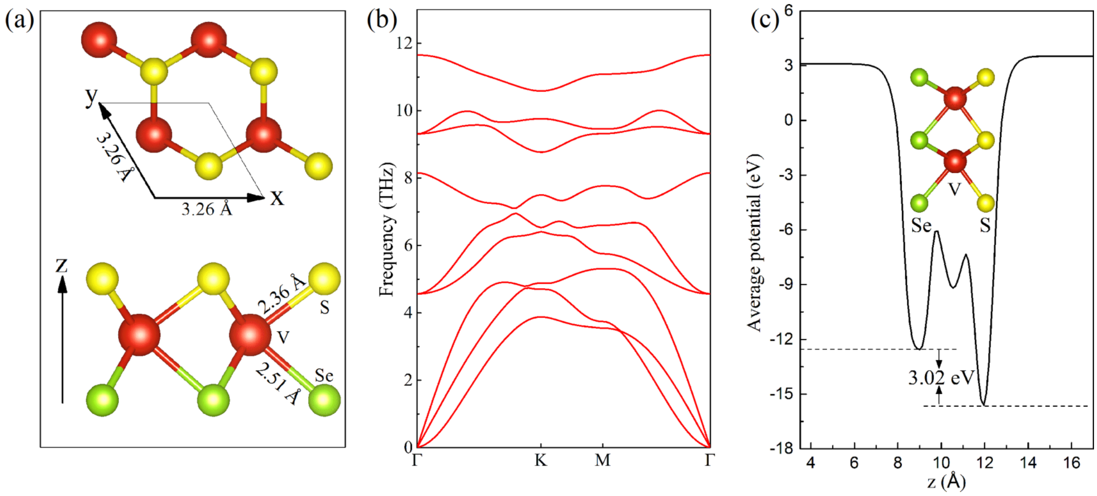

FIG. 1. (a) The top and side views of VSSe. The red, yellow, and green spheres represent the V, S, and Se atoms, respectively. The diamond indicates the unit cell of 2D VSSe. (b) The phonon spectrum of VSSe. (c) The average electric potential along z direction of VSSe.

more tunable in external fields. Therefore, we investigated valley control in VSSe by applying electric field, strain, and changing the magnetization to find the covariation of the electronic, spin, and valley freedoms.

II. METHODS

The first-principles calculation is carried out by using the density-functional theory (DFT) package VASP [26,27]. The generalized gradient approximation functional in Perdew-Burke-Ernzerhof (PBE) form is used [28]. It is found that a $12 \times 12 \times 1$ Γ-centered k mesh and a 400-eV plane-wave truncation energy are sufficient to give convergent results. Spin-orbit coupling (SOC) is taken into account. Considering the deficiency of DFT in estimating the band gap of semiconductors, we calculated the band structure using GW0 approximation to include many-body effects [29]. The monolayer VSSe is simulated by a slab in a supercell with a vacuum layer thicker than 15 Å. Projector augmented wave (PAW) pseudopotential is utilized to describe the interatomic interaction. The criterion for atomic relaxation is 0.001 eV/Å. Since the slab of VSSe is asymmetric, the dipole corrections have been taken into consideration [30]. The phonon spectrum is calculated using PHONOPY [31] to check the dynamical stability of monolayer VSSe. Based on the calculated Bloch states, the Berry curvature of the selected band is calculated through the Kubo formula [32]. The total Berry curvature, anomalous Hall conductivity, and optical conductivity are obtained by WANNIER90 [33]. A fine k mesh of $36 \times 36 \times 1$ is used in WANNIER interpolation. The dielectric function of VSSe is derived from the calculated optical conductivity to study the optical properties.

III. RESULTS AND DISCUSSION

The Janus VSSe is composed of an upper S layer, a lower Se layer, and a middle V layer, as shown in Fig. 1(a). Each V atom has six nearest Se and S neighbors. After optimization of the lattice and the atomic positions, it is found that the lattice constant of VSSe (3.26 Å) [24,25] is between that of VS_2 (3.18 Å) [17] and VSe_2 (3.34 Å) [16]. The V–Se and V–S bond lengths in VSSe are almost the same as they are in VSe_2 and VS_2, respectively. Since V–S bond is much shorter than V–Se bond, it is evident that the mirror symmetry with respect to the V plane in VS_2 and VSe_2 is lost in VSSe [Fig. 1(a)]. There is no imaginary frequency in the calculated phonon spectrum as Fig. 1(b) shows, indicating that VSSe is dynamically stable. By using molecular-dynamics simulations, we further found that VSSe keeps stable and well ordered at the finite temperatures of 300 and 500 K (Fig. S1 in the Supplemental Material [34]). The calculated average electrostatic potential along z axis is quite asymmetric, as depicted in Fig. 1(c). The potential in the vacuum region is flat after dipole corrections (Fig. S3 in the Supplemental Material [34]). We have done Bader charge analysis and found that each V atom loses 1.382e, whereas each Se and S atom obtains 0.605e and 0.777e, respectively, agreeing with the electronegativity order S>Se>V.

Recently, more and more two-dimensional (2D) ferromagnets, such as CrI_3 [35], VSe_2 [36], and $Cr_2Ge_2Te_6$ [37], have been found in experiments, in spite of the Mermin-Wagner theorem. It was assumed that the magnetic anisotropy may play a role to stabilize the long-range magnetic order [35,37,38], which is the case for VX_2 and VXX'. Our calculations show that monolayer H-VS_2 and VSe_2 are ferromagnetic (FM), in consistency with the previous results [15–18]. For VSSe, it is found that ferromagnetic configuration is energetically lower than the antiferromagnetic (AFM) one. Each V atom contributes 1 μ_B magnetic moment. According to the nearest-neighbor Heisenberg model [39], the Curie temperature can be estimated by $3k_BT_c/2 = (E_{\text{AFM}} - E_{FM})/N$, where k_B is the Boltzmann constant, N is the number of magnetic atoms in the supercell, and E_{AFM} and E_{FM} the total energy of AFM and FM configurations, respectively. We compared the total energies of VSSe in FM and various AFM configurations (see Fig. S2 and Table S1 of the Supplemental Material [34]). It is found that E_{FM} is lower than E_{AFM} by 0.216 eV, which corresponds to a Curie temperature of 418 K ($N = 4$), which is between that of VS_2 and VSe_2 [40]. Therefore, VSSe can be ferromagnetic at room temperatures. VX_2 and VXX' have strong SOC, which can lead to magnetic anisotropy.

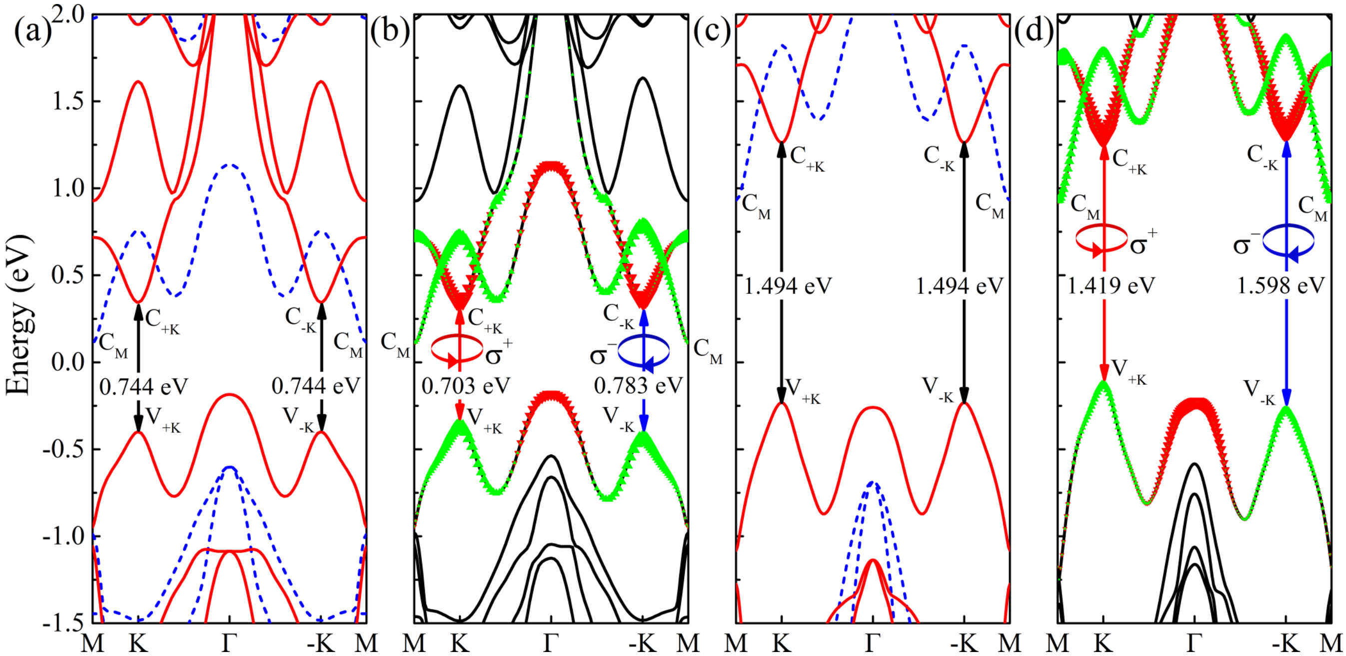

FIG. 2. The PBE (a), (b) and GW (c), (d) band structures of H-VSSe monolayer with (b), (d) and without (a), (c) SOC. The red lines and blue dashed lines in (a), (c) correspond to spin-up and spin-down states. The red and green triangles in (b) and (d) denote the contribution from the d_{z^2} and $d_{x^2-y^2} \pm id_{xy}$ orbitals of V atom, respectively. The arrows between $V_{\pm K}$ and $C_{\pm K}$ denote the valley-selective optical transitions induced by left and right circularly polarized light σ^+ and σ^-.

We calculated the magnetic anisotropic energy of VSe_2 and VSSe and found that their easy axis is in the material plane, whose energy is 0.58 [41,42] and 0.37 meV lower than the perpendicular energy for VSe_2 and VSSe, respectively. The magnetic orientation can be effectively tuned by external fields [43–45] or magnetic substrates [46,47]. It is found that when the orientation of the magnetization is perpendicular to the material plane, VSe_2 will exhibit intriguing properties of ferrovalley, which are under intensive exploration [13,15–18]. To compare the ferrovalley properties of Janus VSSe with those of VSe_2, the perpendicular magnetic orientation is assumed (unless otherwise stated) in the following.

We first calculated the band structure of VSSe with spin polarization but without SOC. It can be found that there is a Dirac valley at each of the K and $-K$ points. Both valence- and conduction-band edges of the valleys are spin-up states, as shown by the two red lines closest to the valley gap in Fig. 2(a). The bands of opposite spins are well separated, which breaks the time-reversal symmetry relation $E_\uparrow(k) = E_\downarrow(-k)$, where the arrows denote the spin directions. In the calculated DFT-PBE band structure, the top of the valence band is located at the Γ point and the indirect band gap for spin-up states is 0.529 eV. The two valleys are degenerate in energy with identical valley gaps of 0.744 eV. After including the many-body effects by using GW approximation, the top of the valence bands is moved from Γ to $\pm K$ points so that the band structure has direct gaps between the spin-up bands at the two valleys. As shown Fig. 2(c), the renormalized band gap is 1.494 eV, almost twice as much as the PBE gap. The dispersion of the bands also changes apparently due to GW corrections. The analysis of the Bloch states at the Dirac valleys shows that the conduction- (C) and valence- (V) band edges near $C_{\pm K}$ and $V_{\pm K}$ are, respectively, d_{z^2} and $d_{x^2-y^2} \pm id_{xy}$ dominant states from V atom, and therefore, their corresponding orbital magnetic moment along the z direction μ_L is $\mu_L(C_{\pm K}) \approx 0$ and $\mu_L(V_{\pm K}) \approx \pm 2\mu_B$, respectively. μ_B is the Bohr magneton.

The band structures taking the SOC into account are shown in Figs. 2(b) and 2(d). One can see that C_K and C_{-K} remain energetically close, whereas V_K is appreciably higher than V_{-K}, thereby reducing the valley gap at K (Δ_K) and increasing the gap at $-K$ (Δ_{-K}). Hence, the valley degeneracy is broken and an evident valley splitting $\Delta = \Delta_{-K} - \Delta_K$ is induced, which is manifested as two splitting peaks in the photoluminescence spectra. Δ has a DFT value of 80 meV. After GW corrections, Δ is significantly increased to 179 meV. The large valley splitting can be ascribed to the ferromagnetism and the strong SOC in V atom between its orbital (μ_L) and spin (μ_S) magnetic moments, which is proportional to $\mu_S \cdot \mu_L$. We calculated the mean value of spin of the states of the valence-band edge and found that $\langle\hat{\sigma}_x\rangle \approx \langle\hat{\sigma}_y\rangle \approx 0$ and $\langle\hat{\sigma}_z\rangle \approx 1$, where $\hat{\sigma}$ is the Pauli operator. Therefore, the spin of the valence-band edge almost remains parallel in the upward direction, producing an effective magnetic field B_{eff} acting on μ_L and inducing an energy shift of $\mu_L B_{\text{eff}}$. As discussed above, the orbital magnetic moment $\mu_L(C_{\pm K}) \approx 0$, and therefore the energy shift $\mu_L(C_{\pm K})B_{\text{eff}} \approx 0$ for conduction valley edges C_K and C_{-K}. In contrast, $\mu_L(V_{\pm K}) \approx \pm 2\mu_B$, leading to an up and down energy shift of $2\mu_B B_{\text{eff}}$ for valence-band edge states V_K and V_{-K}, respectively. The valley gap Δ_K and Δ_{-K} are thus reduced and enlarged by $2\mu_B B_{\text{eff}}$, respectively. As a result, the valley splitting $\Delta = \Delta_{-K} - \Delta_K = 4\mu_B B_{\text{eff}} = 0.23 B_{\text{eff}}$ meV, being close to the experimentally found Δ dependence on the external magnetic field B for MoS_2 and $MoSe_2$, $\Delta = 0.22B$ meV [48,49], where B_{eff} and B are in the unit of tesla. In experiments, an external magnetic field of tens of tesla

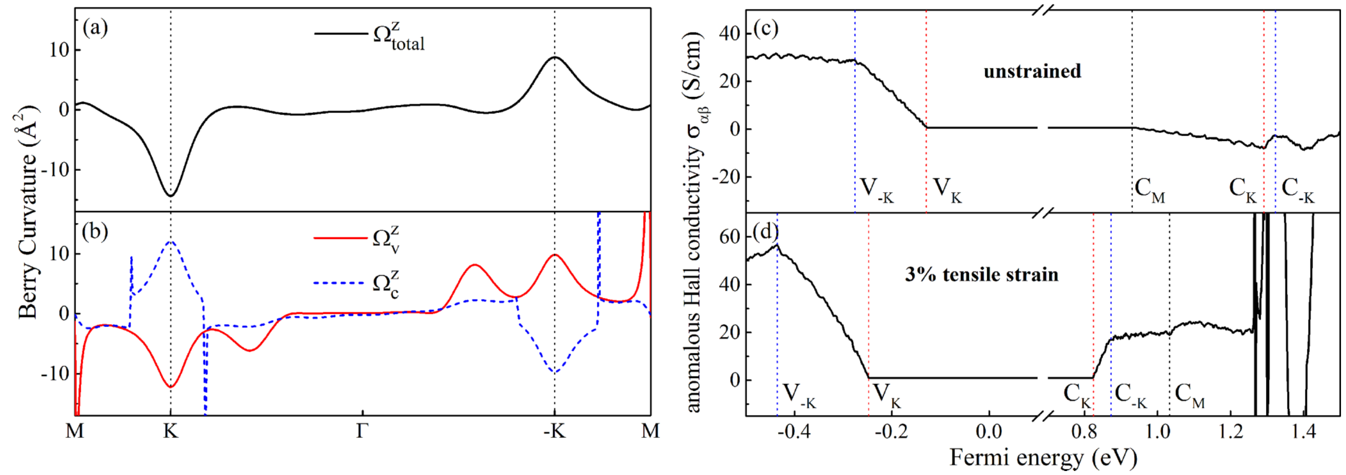

FIG. 3. (a) The z component of the total Berry curvatures of valence bands $\Omega^z_{\mathrm{total}}$. (b) The z component of the Berry curvatures of the valence-band edge Ω^z_V and the conduction-band edge Ω^z_C. (c) The anomalous Hall conductivity dependence on the Fermi level. The points of $C_{\pm K}$, $V_{\pm K}$, and C_M are labeled in the band structures in Fig. 2(d). (d) The anomalous Hall conductivity under 3% tensile strain.

can only induce several meV valley splitting [48,49], whereas ferromagnetic VSSe has a very large valley splitting of 179 meV, which means a $B_{\mathrm{eff}} \approx 800$ T. Suppose one is to create the same valley splitting (179 meV) in MoS_2 and $MoSe_2$ by external magnetic field B, then B should be of similar magnitude ($\sim$800 T). This implies that intrinsic ferromagnetism is much more efficient in producing valley splitting.

We calculated the z component of Berry curvatures $\Omega^z_n(k)$ of the highest valence (V) and the lowest conduction (C) bands according to the Kubo formula [32],

$$\Omega^z_n(k) = \sum_{m\neq n} \frac{2\mathrm{Im}\langle\psi_{nk}|\hat{v}_x|\psi_{mk}\rangle\langle\psi_{mk}|\hat{v}_y|\psi_{nk}\rangle}{[\varepsilon_m(k) - \varepsilon_n(k)]^2}, \qquad (1)$$

where $\hat{v}_x$ and $\hat{v}_y$ are velocity operators along x and y directions, respectively. $|\Psi_{nk}\rangle$ is the calculated wave function of the Bloch state of band n ($= C$ or V) at k point, and ε_{nk} is the energy eigenvalue. For nonmagnetic TMDs, such as MoS_2, the Berry curvature has an odd parity $\Omega^z_n(k) = -\Omega^z_n(-k)$, as dictated by time-reversal symmetry [50]. The calculated Berry curvatures of VSSe are shown in Figs. 3(a) and 3(b). In the intrinsic ferromagnetic field of VSSe, the signs of $\Omega^z_n(K)$ and $\Omega^z_n(-K)$ remain opposite but the magnitudes become different. From Figs. 2(d) and 3(b), one can find that $\Delta_K < \Delta_{-K}$ but $|\Omega^z_n(K)| > |\Omega^z_n(-K)|$ ($n = C$ or V). The inverse relation between the energy gap and the magnitude of Berry curvature can be understood from the Kubo formula [Eq. (1)], which indicates that the largest contribution to $|\Omega^z_n(\pm K)|$ comes from the conduction- and valence-band edges $C_{\pm K}$ and $V_{\pm K}$ due to the inverse dependence on $[\varepsilon_C(\pm K) - \varepsilon_V(\pm K)]^2$, where $\varepsilon_C(\pm K) - \varepsilon_V(\pm K)$ is just the energy gap at $\pm K$. Actually, we found that the Berry curvatures satisfy $\Omega^z_n(K)/\Omega^z_n(-K) \approx -\Delta^2_{-K}/\Delta^2_K$. Interestingly, it is found that this relation still holds during the tuning of the valley splitting by external fields (see below).

If an in-plane electric field $\mathcal{E}_\parallel$ is applied, an anomalous transverse current occurs driven by the Berry curvature $\mathcal{E}_\parallel \times \Omega^z_n(k)$ [50]. In VSSe, Berry curvature is prominent only at the valley edges. As discussed above, $\Omega^z_n(K)$ and $\Omega^z_n(-K)$ have opposite sign and unequal magnitudes, inducing opposite deflection of the valley carriers in transverse direction but at different rate. As a result, a net charge accumulation will develop at one side and a transverse Hall voltage is built. The net charge comes from the same valley with the same spin, which means a simultaneous charge, spin, and valley polarization. In MoS_2, $\Omega^z_n(K) = -\Omega^z_n(-K)$ and hence the valley carriers have the same transverse deflection rate in opposite direction, without inducing charge Hall voltage. We calculated the anomalous Hall conductivity $\sigma^{AH}_{\alpha\beta}$, which is basically determined by the summation of the Berry curvatures of all occupied states over the Brillouin zone. It is found $\sigma^{AH}_{\alpha\beta}$ is always zero for MoS_2 because the odd parity of Berry curvature in MoS_2 cancels its summation over k. In VSSe, the odd parity is broken and the calculation yield a nonzero $\sigma^{AH}_{\alpha\beta}$. When the Fermi level is between the top valence edges of the two valleys V_K and V_{-K}, which corresponds to the case of hole doping, the calculated maximum AHC $\sigma^{AH}_{\alpha\beta}$ is 29.0 S/cm. Between the conduction edges of the two valleys C_K and C_{-K}, the maximum absolute value of $\sigma^{AH}_{\alpha\beta}$ is 7.9 S/cm.

In the nonmagnetic TMDs, such as MoS_2, there is valley-selective circular dichroism, by which one can selectively excite valley carriers at K or $-K$ by using light with opposite circular polarization. To see the effect of ferromagnetism on the optical properties of VSSe, we calculated the interband transition matrix $P^{C,V}_\pm(k) = \langle\Psi_{Ck}|\hat{P}_\pm|\Psi_{Vk}\rangle$, where $\hat{P}_\pm = (\hat{P}_x \pm \hat{P}_y)/\sqrt{2}$ and $\hat{P}$ is the momentum operator. The signs + and – stand for left and right circular polarization, respectively. As shown in Fig. 4(a), we calculated the k-resolved normalized circular polarization $\eta(k) = \frac{|P^{C,V}_+(k)|^2 - |P^{C,V}_-(k)|^2}{|P^{C,V}_+(k)|^2 + |P^{C,V}_-(k)|^2}$, and found that η is nearly ± 1 at $\pm K$ and in their neighborhood, indicating that left (σ^+) and right (σ^-) circularly polarized light can only excite the K and $-K$ valley, respectively, and that the valley-selective circular dichroism persists in the presence of ferromagnetism. If the incident light is unpolarized, which is a superposition of the σ^+ and σ^- components, the K ($-K$) valley only absorbs the σ^+ (σ^-) component.

σ^+ and σ^- peaks can be observed in the polarization-resolved photoluminescence (PL) experiment. In nonmagnetic MoS_2, the two peaks overlap because of the valley

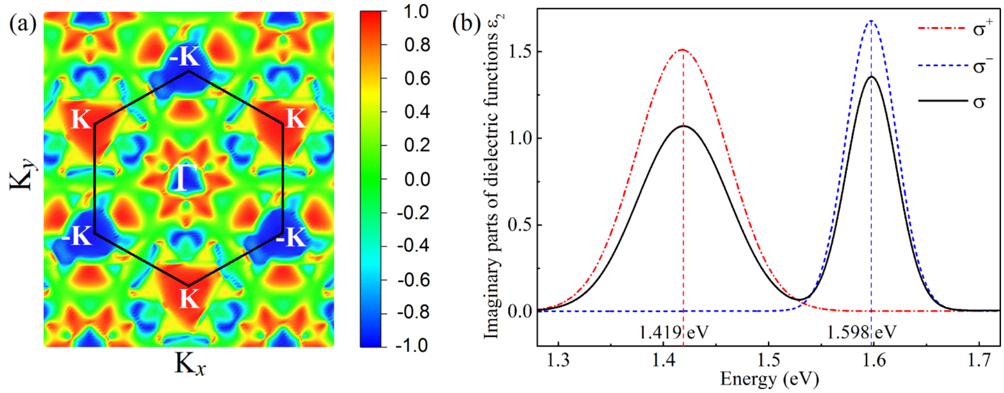

FIG. 4. (a)The circular polarization $\eta(k)$ of the optical transition between the valence- and conduction-band edges in the first Brillouin zone. The hexagon represents the Brillouin zone. The high-symmetry points K, $-K$, and Γ are labeled. The color scale on the right side indicates the values of $\eta(k)$ over the Brillouin zone. (b) The imaginary part ε_2 of dielectric function for left-handed light σ^+, right-handed light σ^-, and unpolarized light σ.

degeneracy. If an external magnetic field is applied, it has been observed in PL spectra that the σ^+ and σ^- peaks are split at a small rate about 0.22 meV/T for MoS_2 and $MoSe_2$ [48,49]. To study the optical properties such as valley Zeeman splitting of the ferromagnetic VSSe, we calculated the imaginary part of the dielectric function, which is related to optical conductivity $\sigma(\omega)$ by $\varepsilon_2(\omega) = 4\pi\sigma(\omega)/\omega$. The optical conductivity is calculated via WANNIER90 with a dense k mesh of $36 \times 36 \times 1$. In Fig. 4(b), one can see that σ^+ and σ^- peak positions correspond to the valley gaps Δ_K and Δ_{-K}, respectively. The splitting between the peaks is 179 meV, which is the same as the calculated valley splitting (GW). Because the σ^+ and σ^- peaks are well split, the excitation energies for K valley E_K and for $-K$ valley E_{-K} differ considerably, making it possible to realize the valley-selective excitation by unpolarized light σ. As known, σ can be decomposed into σ^+ and σ^- components. When the energy of σ is E_K, only the σ^+ component of σ can excite the K valley. However, σ of energy E_K will not excite the $-K$ valley because of the significant excitation energy mismatch between E_K and E_{-K}. Similarly, the unpolarized light of energy E_{-K} can only excite the $-K$ valley. We also calculated the PL spectra of unpolarized light σ, as shown in Fig. 4(b). It can be seen that there are still two well-split peaks located at the same position as the σ^+ and σ^- peaks, which correspond to K and $-K$ valley excitations, respectively. This is not possible for nonmagnetic TMDs since the two valleys are energetically degenerate and have the same excitation energy [7]. In this case, one has to use light of the same energy but with opposite circular polarization to selectively excite the valley carriers.

The lack of time-reversal symmetry and mirror symmetry made VSSe more tunable than nonmagnetic TMDs. We studied the control of valley freedom by magnetization, electric field, and strain. As discussed above, the valley splitting is $4\mu_B B_{\rm eff}$ provided that the orbital magnetic moment (in z direction) is parallel to the effective magnetic field $B_{\rm eff}$. If there is an angle θ between $B_{\rm eff}$ and the orbital magnetic moment [Fig. 5(a)], the valley splitting becomes $4\mu_B B_{\rm eff}\cos\theta$. Therefore, one can rotate the direction of magnetization to tune the valley splitting. In calculation, the spin quantization axis can be aligned to any specified direction. We chose a plane as shown in the inset of Fig. 5(a) and change the spin

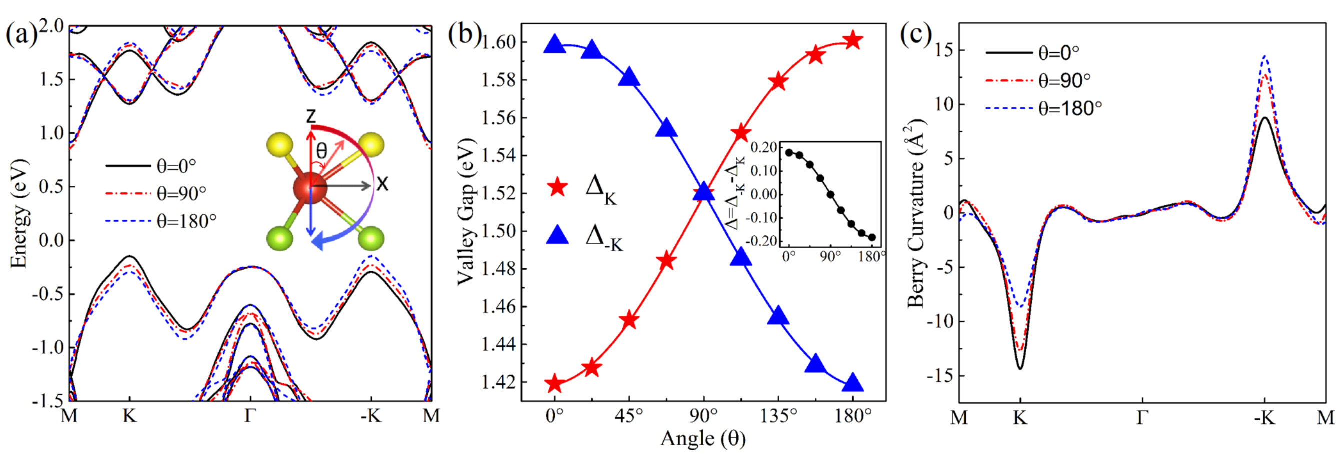

FIG. 5. The tuning of band structures (a), the valley gaps Δ_K and Δ_{-K} (b), and the total Berry curvatures of the valence bands (c) by changing the magnetization angles θ between the magnetic moment and z direction. The inset of (a) indicates the rotation angle and the rotation plane of the magnetization direction. For the definition of x and z directions, please refer to Fig. 1(a). The inset of (b) shows the variation of valley splitting $\Delta(\theta) = \Delta_{-K}(\theta) - \Delta_K(\theta)$ with respect to θ.

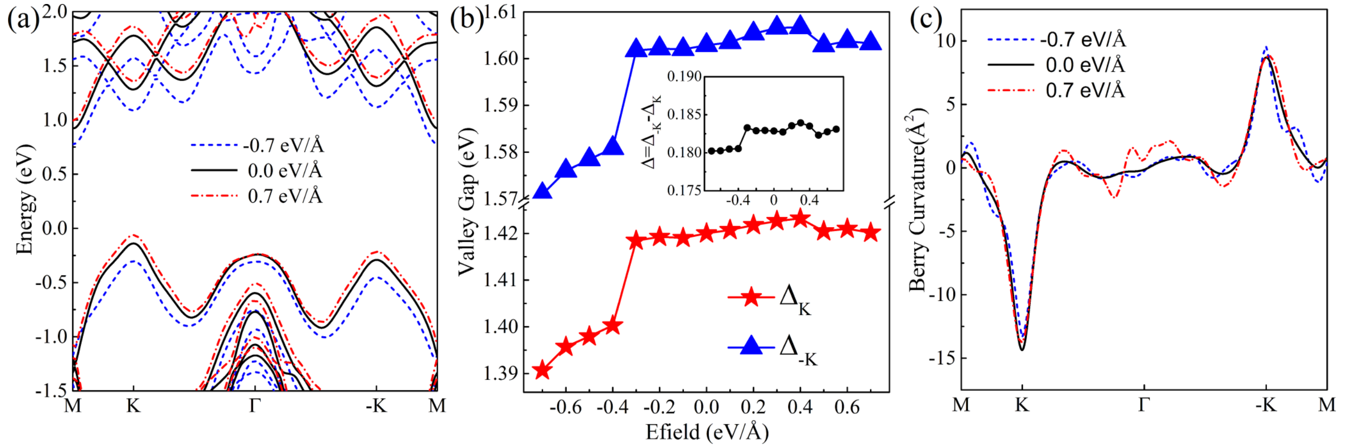

FIG. 6. Electric-field tuning of band structures (a), the valley gaps $\Delta_K(\mathcal{E}_z)$ and $\Delta_{-K}(\mathcal{E}_z)$ (b), and the total Berry curvatures of the valence bands (c). The inset in (b) shows the variation of valley splitting $\Delta(\mathcal{E}_z) = \Delta_K(\mathcal{E}_z) - \Delta_{-K}(\mathcal{E}_z)$ with respect to $\mathcal{E}_z$.

quantization axis within this plane. In this way, the magnetization direction dependent properties can be calculated. We studied the θ-dependent band structure and found that the band gap Δ_K and Δ_{-K} increase and decrease at K and $-K$ valleys, respectively, for $0^\circ \leqslant \theta \leqslant 180^\circ$, as shown in Figs. 5(a) and 5(b). Between 0° and 90°, the valley splitting $\Delta = \Delta_{-K} - \Delta_K$ diminishes but remains positive. When B_{eff} is lying in the plane ($\theta = 90^\circ$), the valley splitting vanishes. With further rotation from 90° to 180°, one can find that valley splitting becomes negative and the magnitude grows until it finally reaches $-4\mu_B B_{\text{eff}}$. Therefore, the valley splitting can be continuously tuned from $4\mu_B B_{\text{eff}}$ to $-4\mu_B B_{\text{eff}}$. We also studied the modulation of Berry curvature Ω_z by changing the magnetization direction. In Fig. 5(c), it can be seen that the Berry curvature difference $|\Omega_z(\mathrm{K})| - |\Omega_z(-\mathrm{K})|$ is largest and zero in magnitude when B_{eff} is perpendicular and parallel to VSSe plane, respectively.

Application of electric field is an effective way to tune the band structure and align the bands. We studied the electric response of VSSe by applying perpendicular electric field $\mathcal{E}_z$. In VSSe, the upper S and the lower Se layers are not mirror symmetric, and consequently the direction of $\mathcal{E}_z$ should make a difference when it points up or down. The GW band structures with $\mathcal{E}_z = 0$ and ± 0.7 eV/Å are plotted in Fig. 6(a). One can see that the band is pushed up in positive $\mathcal{E}_z$ but is pressed down when the $\mathcal{E}_z$.turns negative. The valley gaps Δ_K and Δ_{-K} vary first slowly and linearly with small $\mathcal{E}_z$, and change rapidly in the narrow range around ± 0.4 eV/Å, as shown in Fig. 6(b). But, the valley splitting $\Delta = \Delta_{-K} - \Delta_K$ remains almost invariant. In VSSe, the valley gaps are dependent on the direction of electric field, being enhanced in positive $\mathcal{E}_z$ but reduced in negative $\mathcal{E}_z$. In addition, the magnitude of the gap variation rate also differs in opposite electric field. This is quite different from MX_2 TMDs. Our calculations show that, for instance, the valley gaps of monolayer VSe_2 always grow with $|\mathcal{E}_z|$ regardless of the direction of $\mathcal{E}_z$ due to the mirror symmetry between the two Se layers. We also calculated the Berry curvatures $\Omega_z(\pm\mathrm{K})$ under different $\mathcal{E}_z$, and found the electric field has marginal effect on $\Omega_z(\pm\mathrm{K})$, as shown in Fig. 6(c).

In heterostructures or at different temperatures, VSSe is usually strained. We studied strain effect on the electronic structure of VSSe by calculating the GW band structures under different in-plane strains, as shown in Fig. 7(a). It is

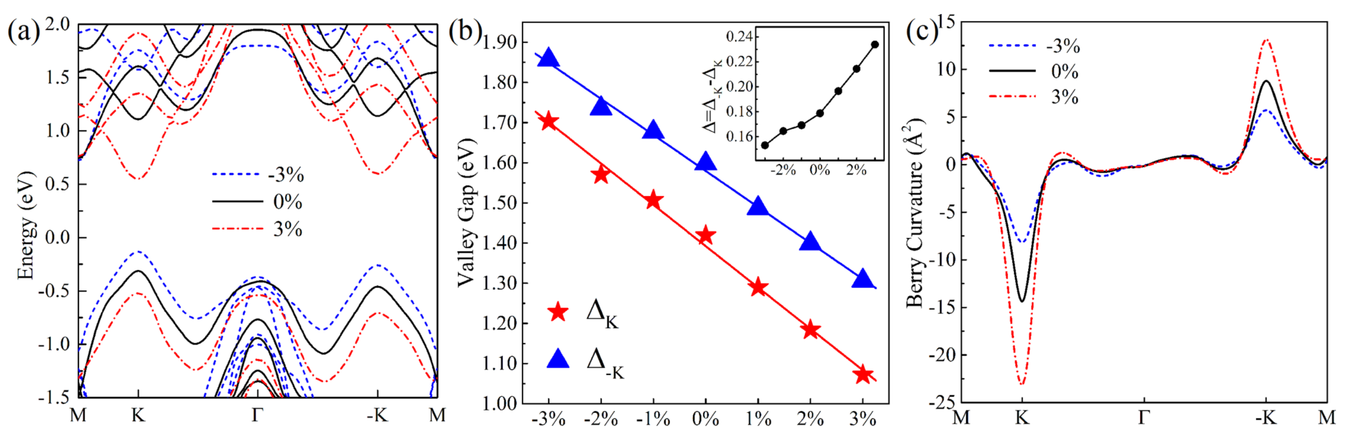

FIG. 7. Strain tuning of band structures (a) and the valley gaps $\Delta_K(\epsilon)$ and $\Delta_{-K}(\epsilon)$ (b) and the total Berry curvatures of the valence bands (c). The inset in (b) shows the variation of valley splitting $\Delta(\epsilon) = \Delta_K(\epsilon) - \Delta_{-K}(\epsilon)$ with respect to ϵ.

found that the tensile strain will move the bands up and the compressive one will press the bands down, with respect to the vacuum level [51]. The strain tuning of the gaps is quite effective. The magnitude of the gap modulation is as large as 0.63 eV for Δ_K and 0.55 eV for Δ_{-K} when the strain is varied between $\pm3\%$. The band gaps $\Delta_{\pm K}$ have linear dependence on strain, being enhanced by stretch and reduced by compression. The slopes of the two lines in Fig. 7(b) indicate that Δ_K has a larger variation rate with respect to strain than Δ_{-K}. Hence, the valley splitting $\Delta = \Delta_{-K} - \Delta_K$ increases under tensile strain and decreases under the compressive strain. The maximum modulation of Δ is 80 meV for $\pm3\%$ strain range. The change of the valley Berry curvature is also considerable [Fig. 7(c)]. The tensile (compressive) strains tend to enhance (reduce) Berry curvatures $\Omega_z(\pm\mathrm{K})$ and also their magnitude difference $|\Omega_z(K)| - |\Omega_z(-K)| = |\Omega_z(K) + \Omega_z(-K)|$. Since the AHC is determined by the summation of the Berry curvatures over the Brillouin zone, and the Berry curvatures are nonzero only around $\pm K$, it is expected that the AHC will be considerably enhanced under the tensile strain as a result of the increase of $|\Omega_z(K) + \Omega_z(-K)|$. With respect to the AHC of the nonstrained VSSe [Fig. 3(c)], the calculated AHC under 3% tensile strain [Fig. 3(d)] is almost doubled when the Fermi level is moved to between V_K and V_{-K} by hole doping, and between C_K and C_{-K} by electron doping. In this way, one can adjust the transverse Hall voltage by strain.

IV. CONCLUSION

In summary, we have studied the valleytronic properties of monolayer Janus VSSe and investigated the control of valley degree of freedom. VSSe is found to be a ferromagnetic semiconductor with strong SOC. The inequivalent Dirac valleys of VSSe have the same spin and are not energetically degenerate due to the breaking of time-reversal symmetry by its ferromagnetism. Compared with the DFT results, the GW renormalized band gap and valley splitting are almost doubled and the valence-band maximum at Γ point is pressed down considerably lower than those at $\pm K$ points, showing strong many-body effects in VSSe. The parity relations $E_n(k) = E_n(-k)$ and $\Omega_n^z(k) = -\Omega_n^z(k)$ are violated. There is a sizable magnitude disparity between the Berry curvatures at K and $-K$, which satisfies $\Omega_n^z(K)/\Omega_n^z(-K) \approx -\Delta_{-K}^2/\Delta_K^2$, and hence results in appreciable anomalous Hall conductivity. The valley-selective circular dichroism persists in ferromagnetism. The calculated optical spectrum features two well-separated peaks and a scheme of valley-selective excitation by unpolarized light is thus proposed. The breaking of symmetries in VSSe makes the valley freedom more tunable. The valley splitting can be continuously modulated and even reversed by rotating the magnetization vector. Unlike the mirror-symmetric MX_2, in which the electric response does not depend on the direction of $\mathcal{E}_z$, VSSe can be bidirectionally tuned when $\mathcal{E}_z$ changes direction due to the mirror-asymmetric Janus structure. Application of lateral strain can effectively modify the band structure. Compressive strains will shift down the bands, reduce the valley gap, and increase the valley splitting appreciably, whereas the tensile strains act oppositely. Accordingly, the variation of Berry curvature is considerable. The AHC can be enhanced by strains and hence the transverse Hall voltage can be effectively controlled by strain.

ACKNOWLEDGMENTS

The authors acknowledge the support of the National Natural Science Foundation of China (Grants No. 11874315 and No. 11874316), the National Basic Research Program of China (Grant No. 2015CB921103), Innovative Research Team in University (Grant No. IRT 17R91), and Hunan Provincial Innovation Foundation For Postgraduate (Grant No. CX20190472).

[1] W. Choi, N. Choudhary, G. H. Han, J. Park, D. Akinwande, and Y. H. Lee, Recent development of two-dimensional transition metal dichalcogenides and their applications, Mater. Today **20**, 116 (2017).

[2] H. Yuan *et al.*, Generation and electric control of spin-valley-coupled circular photogalvanic current in WSe_2, Nat. Nanotechnol. **9**, 851 (2014).

[3] X. Xu, W. Yao, D. Xiao, and T. F. Heinz, Spin and pseudospins in layered transition metal dichalcogenides, Nat. Phys. **10**, 343 (2014).

[4] G. B. Liu, D. Xiao, Y. Yao, X. Xu, and W. Yao, Electronic structures and theoretical modelling of two-dimensional group-VIB transition metal dichalcogenides, Chem. Soc. Rev. **44**, 2643 (2015).

[5] T. Cao *et al.*, Valley-selective circular dichroism of monolayer molybdenum disulphide, Nat. Commun. **3**, 887 (2012).

[6] K. F. Mak, K. He, J. Shan, and T. F. Heinz, Control of valley polarization in monolayer MoS_2 by optical helicity, Nat. Nanotechnol. **7**, 494 (2012).

[7] J. R. Schaibley, H. Yu, G. Clark, P. Rivera, J. S. Ross, K. L. Seyler, W. Yao, and X. Xu, Valleytronics in 2D materials, Nat. Rev. Mater. **1**, 16055 (2016).

[8] T. Olsen and I. Souza, Valley Hall effect in disordered monolayer MoS_2 from first principles, Phys. Rev. B **92**, 125146 (2015).

[9] A. Srivastava, M. Sidler, A. V. Allain, D. S. Lembke, A. Kis, and A. Imamoğlu, Valley Zeeman effect in elementary optical excitations of monolayer WSe_2, Nat. Phys. **11**, 141 (2015).

[10] D. Xiao, G. B. Liu, W. Feng, X. Xu, and W. Yao, Coupled Spin and Valley Physics in Monolayers of MoS_2 and Other Group-VI Dichalcogenides, Phys. Rev. Lett. **108**, 196802 (2012).

[11] W. Yao, D. Xiao, and Q. Niu, Valley-dependent optoelectronics from inversion symmetry breaking, Phys. Rev. B **77**, 235406 (2008).

[12] H. Zeng, J. Dai, W. Yao, D. Xiao, and X. Cui, Valley polarization in MoS_2 monolayers by optical pumping, Nat. Nanotechnol. **7**, 490 (2012).

[13] J. Zhou, Q. Sun, and P. Jena, Valley-Polarized Quantum Anomalous Hall Effect in Ferrimagnetic Honeycomb Lattices, Phys. Rev. Lett. **119**, 046403 (2017).

[14] W. Feng, Y. Yao, W. Zhu, J. Zhou, W. Yao, and D. Xiao, Intrinsic spin Hall effect in monolayers of group-VI dichalcogenides: A first-principles study, Phys. Rev. B **86**, 165108 (2012).

[15] W. Y. Tong, S. J. Gong, X. Wan, and C. G. Duan, Concepts of ferrovalley material and anomalous valley Hall effect, Nat. Commun. **7**, 13612 (2016).

[16] J. Liu, W. J. Hou, C. Cheng, H. X. Fu, J. T. Sun, and S. Meng, Intrinsic valley polarization of magnetic VSe_2 monolayers, J. Phys.: Condens. Matter **29**, 255501 (2017).

[17] H. L. Zhuang and R. G. Hennig, Stability and magnetism of strongly correlated single-layer VS_2, Phys. Rev. B **93**, 054429 (2016).

[18] F. Zhang, W. Mi, and X. Wang, Tunable valley and spin splitting in 2H-$VSe_2/BiFeO_3(111)$ triferroic heterostructures, Nanoscale **11**, 10329 (2019).

[19] A. Y. Lu *et al.*, Janus monolayers of transition metal dichalcogenides, Nat. Nanotechnol. **12**, 744 (2017).

[20] T. Hu, F. Jia, G. Zhao, J. Wu, A. Stroppa, and W. Ren, Intrinsic and anisotropic Rashba spin splitting in Janus transition-metal dichalcogenide monolayers, Phys. Rev. B **97**, 235404 (2018).

[21] F. Li, W. Wei, P. Zhao, B. Huang, and Y. Dai, Electronic and optical properties of pristine and vertical and lateral heterostructures of Janus MoSSe and WSSe, J. Phys. Chem. Lett. **8**, 5959 (2017).

[22] R. Li, Y. Cheng, and W. Huang, Recent progress of Janus 2D transition metal chalcogenides: From theory to experiments, Small **14**, 1802091 (2018).

[23] J. Zhang *et al.*, Janus monolayer transition-metal dichalcogenides, ACS Nano **11**, 8192 (2017).

[24] C. Zhang, Y. Nie, S. Sanvito, and A. Du, First-principles prediction of a room-temperature ferromagnetic Janus VSSe monolayer with piezoelectricity, ferroelasticity, and large valley polarization, Nano Lett. **19**, 1366 (2019).

[25] J. Yang, A. Wang, S. Zhang, J. Liu, Z. Zhong, and L. Chen, Coexistence of piezoelectricity and magnetism in two-dimensional vanadium dichalcogenides, Phys. Chem. Chem. Phys. **21**, 132 (2018).

[26] G. Kresse and J. Furthmüller, Efficient iterative schemes for ab initio total-energy calculations using a plane-wave basis set, Phys. Rev. B **54**, 11169 (1996).

[27] G. Kresse and J. Furthmüller, Efficiency of ab-initio total energy calculations for metals and semiconductors using a plane-wave basis set, Comput. Mater. Sci. **6**, 15 (1996).

[28] J. P. Perdew, K. Burke, and M. Ernzerhof, Generalized Gradient Approximation Made Simple, Phys. Rev. Lett. **77**, 3865 (1996).

[29] M. Shishkin and G. Kresse, Implementation and performance of the frequency-dependent GW method within the PAW framework, Phys. Rev. B **74**, 035101 (2006).

[30] L. Bengtsson, Dipole correction for surface supercell calculations, Phys. Rev. B **59**, 12301 (1999).

[31] A. Togo and I. Tanaka, First principles phonon calculations in materials science, Scr. Mater. **108**, 1 (2015).

[32] D. J. Thouless, M. Kohmoto, M. P. Nightingale, and M. den Nijs, Quantized Hall Conductance in a Two-Dimensional Periodic Potential, Phys. Rev. Lett. **49**, 405 (1982).

[33] A. A. Mostofi, J. R. Yates, G. Pizzi, Y.-S. Lee, I. Souza, D. Vanderbilt, and N. Marzari, An updated version of WANNIER90: A tool for obtaining maximally-localised Wannier functions, Comput. Phys. Commun. **185**, 2309 (2014).

[34] See Supplemental Material at http://link.aps.org/supplemental/10.1103/PhysRevB.101.245416 for molecular dynamics simulation, energies of FM and AFM configurations, band structures with and without dipole corrections, and formation energies of VSSe and MoSSe.

[35] B. Huang *et al.*, Layer-dependent ferromagnetism in a van der Waals crystal down to the monolayer limit, Nature (London) **546**, 270 (2017).

[36] M. Bonilla *et al.*, Strong room-temperature ferromagnetism in VSe_2 monolayers on van der Waals substrates, Nat. Nanotechnol. **13**, 289 (2018).

[37] C. Gong *et al.*, Discovery of intrinsic ferromagnetism in two-dimensional van der Waals crystals, Nature (London) **546**, 265 (2017).

[38] B. Shabbir, M. Nadeem, Z. Dai, M. S. Fuhrer, Q.-K. Xue, X. Wang, and Q. Bao, Long range intrinsic ferromagnetism in two dimensional materials and dissipationless future technologies, Appl. Phys. Rev. **5**, 041105 (2018).

[39] J. Kudrnovský, I. Turek, V. Drchal, F. Máca, P. Weinberger, and P. Bruno, Exchange interactions in III-V and group-IV diluted magnetic semiconductors, Phys. Rev. B **69**, 115208 (2004).

[40] H. Pan, Electronic and magnetic properties of vanadium dichalcogenides monolayers tuned by hydrogenation, J. Phys. Chem. C **118**, 13248 (2014).

[41] S. Feng and W. Mi, Strain and interlayer coupling tailored magnetic properties and valley splitting in layered ferrovalley 2H-VSe_2, Appl. Surf. Sci. **458**, 191 (2018).

[42] H.-R. Fuh, C.-R. Chang, Y.-K. Wang, R. F. Evans, R. W. Chantrell, and H.-T. Jeng, New-type single-layer magnetic semiconductor in transition-metal dichalcogenides VX_2 (X = S, Se and Te), Sci. Rep. **6**, 32625 (2016).

[43] J. Qi, X. Li, Q. Niu, and J. Feng, Giant and tunable valley degeneracy splitting in $MoTe_2$, Phys. Rev. B **92**, 121403 (2015).

[44] A. Chernyshov, M. Overby, X. Liu, J. K. Furdyna, Y. Lyanda-Geller, and L. P. Rokhinson, Evidence for reversible control of magnetization in a ferromagnetic material by means of spin–orbit magnetic field, Nat. Phys. **5**, 656 (2009).

[45] N. Miyata and B. Argyle, Magnetocrystalline anisotropy of single-crystal europium oxide, Phys. Rev. **157**, 448 (1967).

[46] C. Zhao *et al.*, Enhanced valley splitting in monolayer WSe_2 due to magnetic exchange field, Nat. Nanotechnol. **12**, 757 (2017).

[47] D. Zhong *et al.*, Van der Waals engineering of ferromagnetic semiconductor heterostructures for spin and valleytronics, Sci. Adv. **3**, e1603113 (2017).

[48] D. MacNeill, C. Heikes, K. F. Mak, Z. Anderson, A. Kormanyos, V. Zolyomi, J. Park, and D. C. Ralph, Breaking of Valley Degeneracy by Magnetic Field in Monolayer $MoSe_2$, Phys. Rev. Lett. **114**, 037401 (2015).

[49] Y. Wu, C. Shen, Q. Tan, J. Shi, X. Liu, Z. Wu, J. Zhang, P. Tan, and H. Zheng, Valley Zeeman splitting of monolayer MoS_2 probed by low-field magnetic circular dichroism spectroscopy at room temperature, Appl. Phys. Lett. **112**, 153105 (2018).

[50] D. Xiao, W. Yao, and Q. Niu, Valley-Contrasting Physics in Graphene: Magnetic Moment and Topological Transport, Phys. Rev. Lett. **99**, 236809 (2007).

[51] D. Zhang and S. Dong, Challenges in band alignment between semiconducting materials: A case of rutile and anatase TiO_2, Prog. Nat. Sci. **29**, 277 (2019).